PCCP

Accepted Manuscript

This is an *Accepted Manuscript*, which has been through the Royal Society of Chemistry peer review process and has been accepted for publication.

Accepted Manuscripts are published online shortly after acceptance, before technical editing, formatting and proof reading. Using this free service, authors can make their results available to the community, in citable form, before we publish the edited article. We will replace this *Accepted Manuscript* with the edited and formatted *Advance Article* as soon as it is available.

You can find more information about *Accepted Manuscripts* in the **Information for Authors**.

Please note that technical editing may introduce minor changes to the text and/or graphics, which may alter content. The journal's standard **Terms & Conditions** and the **Ethical guidelines** still apply. In no event shall the Royal Society of Chemistry be held responsible for any errors or omissions in this *Accepted Manuscript* or any consequences arising from the use of any information it contains.

www.rsc.org/pccp

Journal Name

ARTICLE

Bilayered graphene as platform of nanostructures with folded edge holes

L. A. Chernozatonskii,[a,b] V. A. Demin[a] and Ph. Lambin[c]

Stability and electronic properties of new AB-stacking and moiré bilayer graphene superlattices with closed edge nanoholes are studied using DFT method calculations. The closing of the edges is made by C-C bonds that form after folding the borders of the holes. Superlattices with periodic hexagonal symmetry are considered with more details. The electronic band structure of the nanomeshes has metallic to semiconductor characteristics, depending not only on the size of the holes and the distance between them, but also on the hole shape. Bilayered graphene is considered as platform for the engineering of nanostructures with folded edge holes

Introduction

Graphene is a marvelous material whose characteristics have more than amply be described in the literature. It has drawbacks, however, which have the same origin as its remarkable properties. With its intrinsic zero band gap, on the one hand, graphene is neither a metal nor a semiconductor. Due to the linear dispersion of the graphene energy bands near the Fermi level, on the other hand, a potential barrier induced by a gated electrode is transparent to electrons arriving at normal incidence. These two effects are unwanted for most applications of graphene in nanoelectronic devices. A lot of efforts are therefore put worldwide to modify the intrinsic properties of graphene without affecting much its remarkable useful characteristics such as a high carrier mobility. These modifications can be physical (effect of the substrate that holds graphene or application of a magnetic field), chemical (doping, functionalization), geometrical (finite width, mechanical deformation) or structural.[1-10] The present work belongs to the last cited category of modification, namely the perforation of holes to create a superstructure at a larger scale than the atomic lattice parameter.

Two-dimensional (2D)[1-6] and 1D one-dimensional[7-9] graphene superstructures (SS) are attracting a growing interest primarily for their semiconducting properties contrasting the graphene ones[10]. Many SS options proposed, and partially implemented today, consist of graphene nano-meshes (GNM) or antidot lattices.[3-6,11-15] For example,[16-18] arrays of holes can be fabricated in graphene by using a thin anodic aluminum oxide etching mask, electron irradiation with energies below the knock-on damage threshold of graphene, and etching in oxygen-nitrogen atmosphere. The behavior of the gap value E_g is directly dependent on the distance between the nanoholes, their shape and size.[3-6,11-13] If GNMs are promising for filtration of molecules[18] for instance, they can also find applications in nanoelectronic devices. In particular, they can sustain high electric currents and exhibit negative differential conductance.[19] In addition, they can be used in field-effect transistors with enhanced properties[20] and supercapacitor electrodes.[21]

The motivation for conducting research on bilayer graphene nanomeshes is manyfold: 1) this form of perforated graphene does not contain chemically active atoms on the hole edges and then its hole edges are less reactive than the ones in single GNMs and are therefore more stable; 2) it should present an electron mobility better than in single-layer GNMs because this sp^2 system can be viewed as a multiply connected surface that has no boundaries, the electrons move freely through the surface as in the case of carbon nanotubes with small number of topological defects; 3) a bilayer GNM can have semiconductor or metallic properties depending on its structure.

Bilayer AB- or AA-stacking of graphene is attracting a growing attention due to its unusual electronic structure compared to that of single graphene.[22] Furthermore, in the case of moiré packing the related periodic superlattice may give rise to many cones in the electronic spectrum.[23] Recently we proposed «honeycomb» nanomesh structures based on bilayer AA-stacking graphene with hexagonal holes.[24-26] It was shown that the zig-zag edges of face-to-face holes lead to covalent bridges resulting in an energetically favorable closed structure with sp^2 topologically connected layers. Thus we obtained much connected topological surface or quasi 2D schwartzite which

a. Emanuel Institute of Biochemical Physics of RAS, Kosygin st. 4, 119334 Moscow, Russian Federation.
b. Chemistry Physics School, Plekhanov Russian University of Economics, 36 Stremyanny per., 117997 Moscow, Russian Federation.
c. Department of Physics, University of Namur, 61 Rue de Bruxelles, 5000 Namur, Belgium.
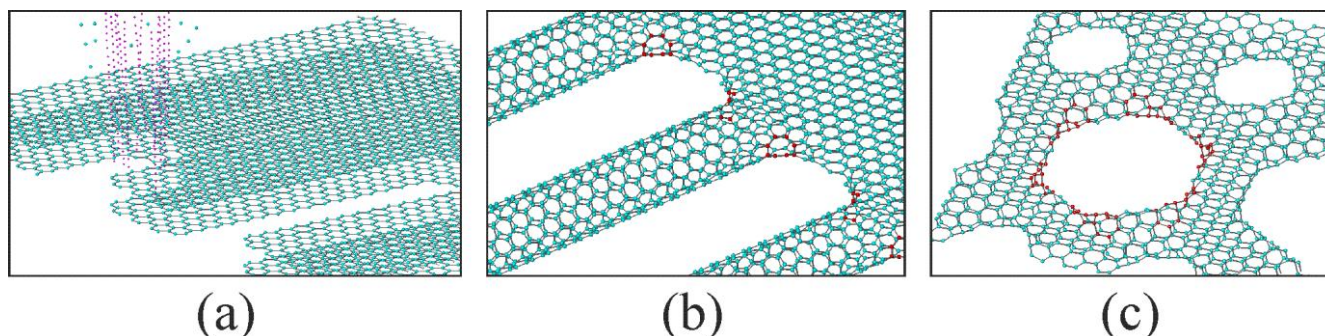
Fig. 1 Schematic construction of bilayered graphene nanomeshes: preparation by cutting along zig-zag directions AA- (or AB-) stacking bi-G using electron beam (a), and transformation (b, c) during reaction of covalent bonding of C-atom pairs of two zig-zag edges into bi-G nanomesh with folded edge holes. In the GAA case (b) red circles show C-atom octagons at the corners of the 120° graphene fold conversion[24-26,35]; in the case of AB-stacking brown circles show pairs of heptagons at 120° corners at the intersection of one Z direction with another Z of graphene fold.

was proposed first in Ref.[27] as analog 3D carbon schwarzites.[28-29] However the AB-stacking and moiré graphene systems with interconnected holes (hereafter called «folded» holes) have not yet been studied in details, though some bilayered G_{AB} SS with unfolded holes have been recently investigated.[30-31] It is only very recently that folded holes in bi-graphene producing have been reported.[32]

Here we focus our attention mainly on new nanomeshes of bilayer AB-stacking Bernal graphene with «round» folded holes which are triangle-like holes in each layer. Their electronic structures are compared with the ones of single graphene and AA-stacking nanomeshes which geometry similar to the AB-stacking one. It is known that the chemical reactivity of graphene edges depends of their configurations: the zigzag (Z) edge atoms are more reactive than atoms of an armchair edge.[33] Therefore, we will consider nanomesh SSs with Z edge holes only.

It is possible to prepare a structure with holes whose edges resemble smooth graphene folds by putting electron beam on bi-G surface[32-38] as it is shown in Fig. 1a. Thus a fully continuous unbroken honeycomb bilayered structure of sp^2 – hybridized carbon atoms (Fig. 1b,c) is formed. By moving the e-beam spot, elongated holes can be obtained – Fig.1 a,b. «Round» holes– Fig. 1c - are obtained by using local e-beam irradiation. The smooth and closed boundaries in the holes should affect scattering of charge carriers much less than in single GNMs.

This paper contains the following parts: calculation methods; how «round» holes with closed edges can be constructed in AB-stacking graphene; architectonics of bi-G hexagonal SS nanomeshes including comparison of the G_{AA} and G_{AB} meshes with GNMs of similar geometry; hexagonal bi-G_{AB}NMs with «oval» closed edge holes; moiré bi-G nanomeshes with closed edges of the holes on AB- and AA-stacking regions; main electronic parameters of the considered bi-G nanomeshes; nanoengeeniring on the base bi-GNMs; summary.

Calculation methods

First-principle calculations within the framework of density functional theory were performed using SIESTA Package.[39] *Ab-initio* LDA DFT calculations with standard norm-conserving pseudo-potentials, flexible numerical LCAO double zeta + polarization orbital basis sets were used. The 2D system is separated from its periodic images by a vacuum distance of 10 Å. The exchange-correlation potential due to Perdew–Zunger[40] was incorporated at the level of the local density approximation (LDA) for electronic structure calculations. To calculate the equilibrium atomic structures, the Brillouin zone (BZ) was sampled according to the Monkhorst–Pack scheme[41] with a *k*-points density 0.06 Å^{-1}. Structural relaxation was carried out until the change in the total energy was less than 10^{-4}eV, or forces acting on each atom were less than 10^{-3} eV Å^{-1}. This method has the drawback to underestimation of the band gap of about 25-40%.[42] Nevertheless, its qualitative predictive ability suffices for the present exploratory work.

Results and discussion

**How «round» holes with closed edges can be construct in AB-stacking graphene**
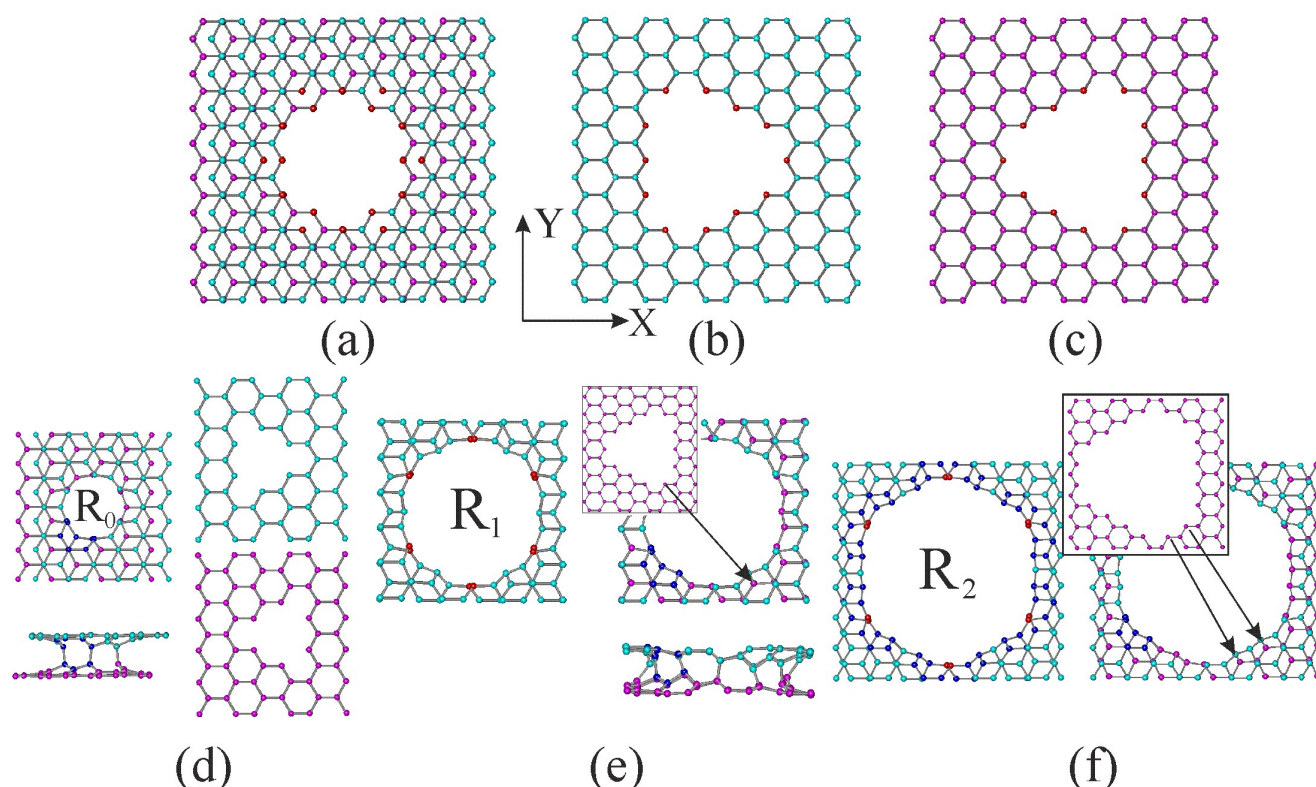
Fig. 2 Details on the construction of bilayered graphene GAB with «round» holes R_q, q=0, 1, 2: (a) the hole R_1 is represented before interconnecting the edges by covalent bonds liking corresponding pairs of atoms shown in red, (b and c) triangular holes in the top G_A layer and the bottom G_B layer whose superposition gives (a); (d) the torus-like hole R_0 has 6 joined octagons (8 atoms drawn in blue belong to the one of them - 5 atoms in G_A and 3 atoms in G_B); right-hand side: green G_A and violet G_B layers after extraction of 4x2 close atoms; (e) the hole R_1 after extraction of 44 close atoms has 6 pairs of joined heptagons (one of them is shown in blue) and 6 pairs of bounded atoms located one above another in bi-graphene (shown in red in the left-hand side structure), between them, pairs of atoms are situated on opposite Z- edges of G_{AB}; (f) hole R_2 after extraction of 104 atoms has 12 heptagons interconnected two by two (blue atoms together with 6 bounded pairs of red atoms situated one above another). G_A layer is indicated by cyan atoms, the G_B layer by violet atoms in (c-e). Bottom drawings in (d) and (e) are side views of the corresponding folded holes $R_{0,1}$.The arrows in (e) and (f) show the Z connected atoms in a corner of the holes (one such atom in each corner of R_1, two in each corner of R_2).

Bilayer graphene is slightly more stable with the Bernal lattice (G_{AB}) than with the AA-stacking configuration G_{AA} (where each atom in one layer is located exactly over an atom of the other layer).[43] We constructed a hole using connection of Z edges mainly along the same way as in Refs.[34-35] and considered first G_{AB} superlattices with hexagonal-like «round» holes. The principle of their formations is shown in Fig.2. When narrow electronic beam is focused on G_{AB} surface with ≈1nm size spot it can be form a «round» hole by, for example, knocking 22-atoms out of G_{AB} (11 atoms from each layer, Fig. 2a). The 12 pairs of edge atoms (each atom in one layer is located close over the atom of the other layer) are connected and form all sp^2 smooth folded hole with radius R_1 (one Z atom in each corner) - Fig. 2e. The hole in the top layer has a triangular form as a truncated triangle similar to the one considered earlier in GNMs.[4,44,45] The hole in the bottom layer has the same shape but is rotated by 180° - Fig. 2 b,c. By reducing the spot size of the focused electron beam, 4x2 atoms can be knocked on after what a smallest hole R_0 can be formed (Fig. 2d), where two pairs of atoms on zig-zag sectors lying between two pairs of

atoms located exactly one above another can be connected and all of them organize the folded hole.

«Round» hexagonal holes in AB-stacking graphene are shown In Fig. 2 d-f. The insets in Fig. 2e-f show truncated triangular holes after extraction of N(q) atoms from each graphene sheet for q= 1 and 2. Hole radius $R_q=(q+1)a_{C-C}\sqrt{3}$ is the distance between two close red pairs of atoms in units of $a_{C-C}\approx1.42$Å. For each q, the R_{q+1} hole follows from R_q by the addition of one hexagon row along the zigzag sides of the truncated triangular. Each side of the truncated triangle hole R_q increases by $a_{C-C}\sqrt{3}$ when q increases by one.

Each torus-like hole has topological defects: 6 octagons in the R_0 hole, and 12 heptagons in $R_q>1$ holes. In these 2D schwarzites the number of non-hexagonal rings in each inner torus region must satisfy a relation extracted from Euler theorem formula: $n_7+2n_8 = 12$, where n_7 and n_8 are the numbers of heptagons and octagons in the hole structure. The R_1 hole is organized from R_0 by extracting 36 atoms close to the border. The next R_2 hole is organized in a similar way after 60 atoms are removed from the border of the hole R_1 - Fig. 2f.
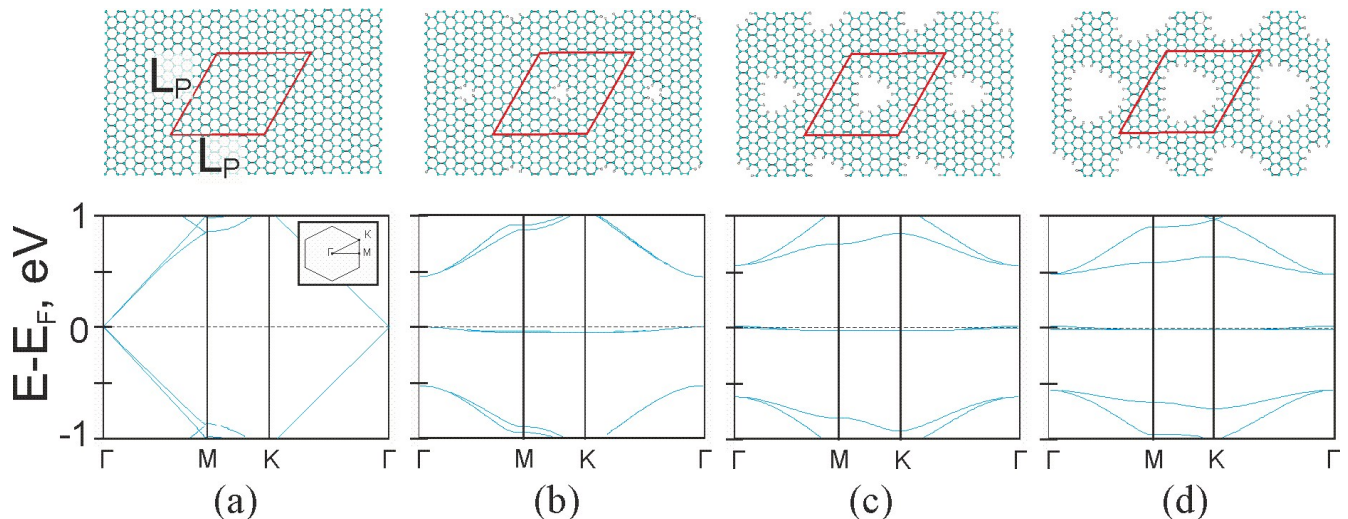
Fig. 3 Atomic structures of hexagonal SSs and their electronic band structures: (a) graphene, (b-d) G{5,t_0}, G{5,t_1}, G{5,t_2} nanomeshes with triangular or truncated triangular holes, respectively. UC (red rhombus) has parameter $L_5 \approx 5 \times 3a_{C-C}$; the inset shows first BZ scheme, H-atoms are adsorbed on the hole edges.

The holes R_q of larger radius (q>2) can be generated in a similar fashion with formation of truncated triangles in each graphene layer. It is easy to obtain a simple recurrence formula between the numbers of extracted atoms: $N_{ext} = 2N(q)$, $N(q) = N(q-1) + 6(2q+1)$ were q≥1, $N(0)=4$. For example, $N_{ext}(2) = 104$ ($N(2) = (22+30)$ for the «round» R_2 holes of G_{AB} SS.

Architectonics of bi-graphene nanomeshes

First we will consider single-layered and AA bilayered meshes with the same geometry as triangle-like hole structure in AB «round» hole - Fig. 2. Next, the electronic properties of hexagonal G{L_p,t_q} meshes (with similar truncated triangle holes t_q^{45}) will be compared with new hexagonal superlattices G_{AA}{L_p,t_q} and G_{AB}{L_p,R_q} on the example of hexagonal unit cell (UC) parameter $L_5 = 5 \times 3a_{C-C}$ along armchair direction (see Fig. 3). According to the rule derived for nanomeshes (see eq. (3) in

Ref.[6]) we obtain semiconductor behavior for all G{L_p,t_q} NMs with a gap $E_g \sim$ 1eV. Besides that, all NMs with translation vectors codirectional to «armchair» are semiconductors.[6] However, due to the triangular shape of the holes, we obtain a flat or dispersionless band near E_F induced by electron localization close to hole corners (see Refs.[4-13]) for the meshes G{5,t_q}. The situation is similar to hydrogenated graphene SS with hydrogen atoms[5,6] adsorbed on the very same C atoms than those that were extracted here. The band structure depends weakly of the hole size.

Another semimetal behavior is obtained when we consider the nanomeshes G_{AA}{5,t_q} constructed from two connected meshes G{5,t_q} - Fig. 4. Here the C atom bonds near the holes are strained and, therefore, electrons remain somewhat localized near the holes and form minizones near E_F. This is not full localization, however, for the electrons can move from one layer to the other through sp^2 hole edge bonds that stitch the layers together. This topology changes the band structure
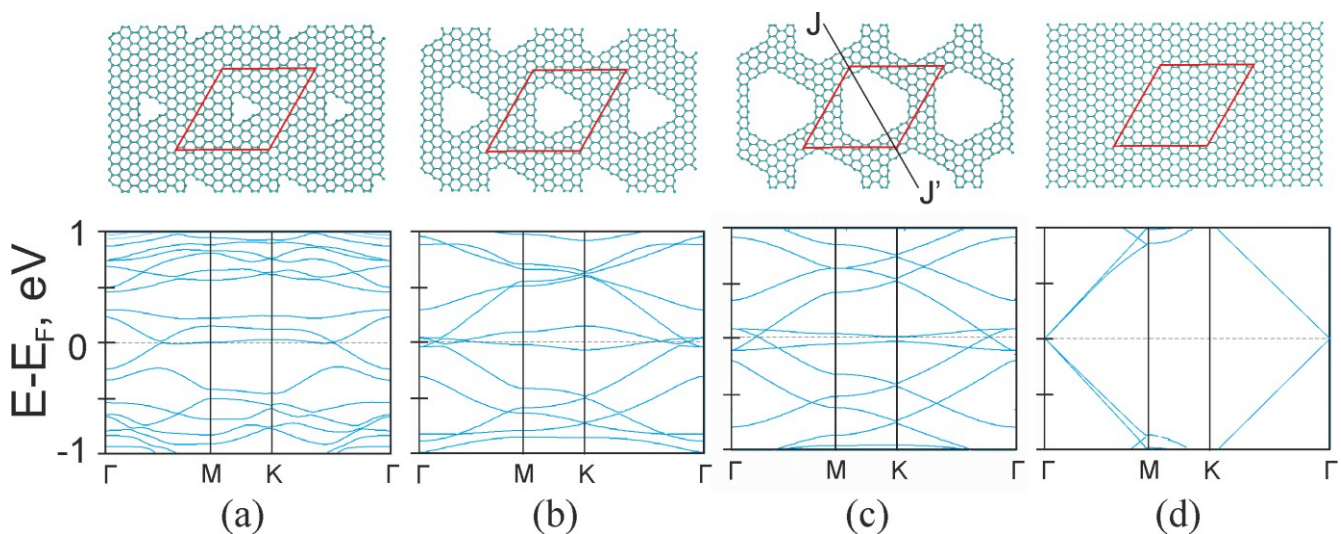
Fig. 4 Atomic structure and electronic band structure of nano-meshes obtained from two meshes G{5,t_q} in AA-stacking with folded holes: (a) G_{AA}{5,t_0}, (b) G_{AA}{5,t_1} and (c) G_{AA}{5,t_2}. For comparison purpose, (d) represents corresponding graphene SS.

shown in Fig. 3b. In the case of mesh $G_{AA}\{5,t_0\}$ (Fig. 4a), there are two band crossings (Dirac points) in the spectrum with a flattened branch between the two Dirac points. In the mesh $G_{AA}\{5,t_1\}$ (Fig. 4b), electrons can pass from one layer to another through their small-strained C-C bonds of the torus parts. Therefore, there are two Dirac points in the spectrum, which is the result of electron moving in different semimetal ribbon-like parts of the 2D superlattice. The structure $G_{AA}\{5,t_2\}$ has larger holes than in $G_{AA}\{5,t_1\}$ - Fig. 4c. Nevertheless C-C bonds remain strained, and some localization of electrons remains close to the holes. Remarks that we have collapsed (8,8), (6,6) and (4,4) CNT fragments between the holes in the $G_{AA}\{5,t_0\}$, $G_{AA}\{5,t_1\}$ and $G_{AA}\{5,t_2\}$, respectively.

The holes in $G_{AA}\{5,t_0\}$ are closed by octagons that conserve two sublattices like in graphene. This topology preserves part of the electron-hole symmetry of the band structure of this nanomesh, which is required for the existence of Dirac cones in the band structure.

A possible reason for the appearance of two Dirac points in the band structures of the meshes $G_{AA}\{5,t_q\}$ is the twofold symmetry of the holes (see direction J-J' Fig. 4). The Dirac points do not stay at high-symmetry points of the SS Brillouin zone. There is no gap opening, because the structures possess an overall symmetry in spite of the holes. Thus we observe the presence of massless charge carriers near the Dirac points in these structures. However the slopes of the main electron-hole branches in the Dirac cones decrease compared to graphene monolayer (see Figs. 4 a-d) and so do the Fermi velocities. This is due to the fact that the C-C bonds in octagons of the nano-holes are strained and angles between bonds in folded parts are smaller 120° (for example, some lengths $a_{C-C} \approx 1.45$-1.47Å and some angles $\approx 112°$ in the mesh $G_{AA}\{5,t_1\}$). Therefore charge carriers are localized near these topological features of the bi-graphene meshes. The degeneracy of branches in graphene with the supercell parameter L_5 (Fig. 4d) splits partially in triangular nanomeshes (Fig. 4a-c). As a consequence of this Dirac cones are deformed near Fermi level. The Fermi velocities v_{Fi} are smaller than $v_F = 1 \times 10^6$ m/s in 2D graphene: $v_{F0,1,2}/v_F = 0.67$, 0.53, 0.75, respectively. This spectrum behavior is greatly different from that of the semiconductor meshes biG_{AA} with similar hexagonal structures and hexagonal holes.[26]

AB-stacking cases

In this Section, we study folded nanomeshes obtained from two AB-stacking $G_{AB}\{5,R_q\}$ constructed from single nanomeshes, which are rotated one another by 180° as shown in Fig. 2. First, meshes with small holes and large distances between neighbor holes are considered – Fig. 5 a,b.

The meshes $G_{AB}\{5,R_q\}$ have strained C-C bonds in their hole torus regions. The $G_{AB}\{5,R_0\}$ structure (Fig. 5a) reveals metallic character ,which can be related to reconstructed bonds of atoms near narrow holes - this is indicated in the MK region by flat bands related to electron localization near the hole. The $G_{AB}\{5,R_1\}$ structure is semiconductor with and indirect gap $E_g = 0.21$ eV. Increasing the hole even further (104 atoms
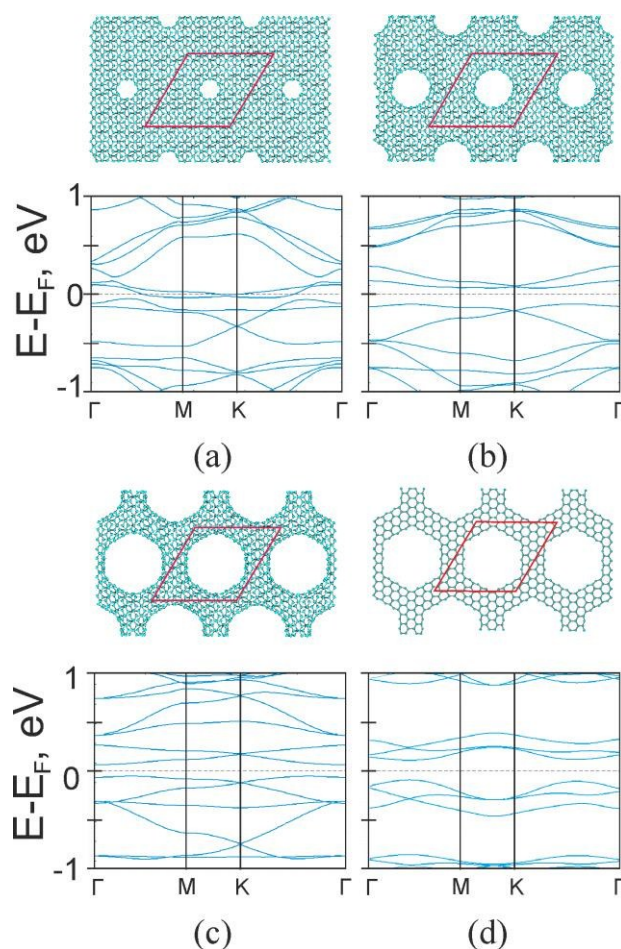
Fig. 5 Geometry and electronic structure of G_{AB}NMs with hexagonal SS parameter $L_5 \approx 2$nm: (a) n-type carrier metal $G_{AB}\{5,R_0\}$ and semiconductors: (b) $G_{AB}\{5,R_1\}$ and c) $G_{AB}\{5,R_2\}$ with $E_g = 0.21$ and 0.19 eV, respectively. For comparison purpose, (d) represents the nanomesh $G_{AA}\{5,h_2\}$, $E_g = 0.21$eV.

removed) leads to the $G_{AB}\{5,R_2\}$ structure It has a band gap 0.19 eV. The optimized UC parameter L decreases slightly from 21.25 to 20.99Å as the number of atoms in the UC decreases and the regions between holes become less flat. Because of all nanomeshes $G_{AB}\{L_p,R_q\}$ have chemically low active sp^2 - atoms on the hole edges, there are no magnetic atoms on the hole corners in contrast with single layered $G\{L_p,t_q\}$ (see Fig. 3, and Refs.[11,45]). There is no strong electron localization near the nanomeshes holes shown on the Fig. 5b,c. Therefore they have band gaps of the order of 0.2 eV, not as big as in the case of single layered meshes $G\{5,t_q\}$ (compare with Fig. 3) because of some leakage of electrons through folded hole edges.

We compare now nanomeshes $G_{AB}\{5,R_2\}$ and $G_{AA}\{5,h_2\}$ with the same parameter L_5. The mesh $G_{AA}\{5,h_2\}$ has a smaller number of C-atoms (192) than in the $G_{AB}\{5,2\}$ UC (196). In the AA-stacking mesh the presence of symmetrically arranged atoms leads to generation of two mini-zones formed by tree π-branches near E_F and separated by the gap 0.23 eV (Fig. 5d). These mini-zones, in turn, are separated the gaps (E ≈ 0.7eV from the following permitted zones. The mesh $G_{AB}\{5,R_2\}$ has

ARTICLE

Journal Name
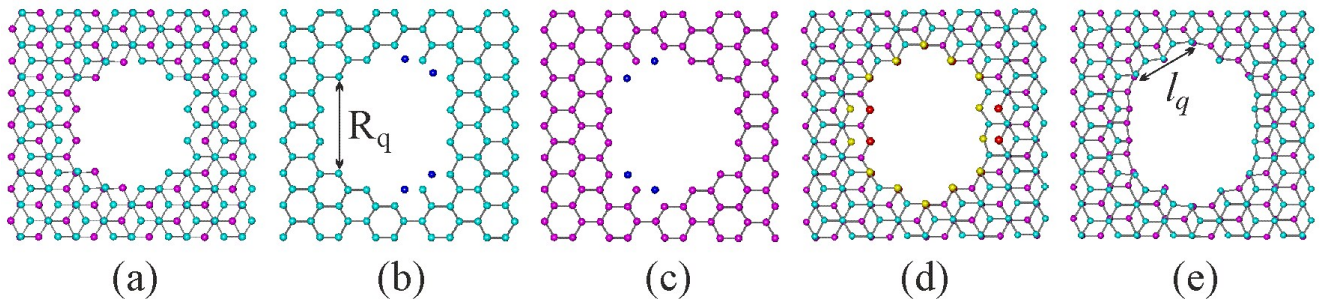
Fig. 6 Details of the construction of AB-stacking bilayer graphene with «oval» hole O_2: preliminary view of hexagonal holes with radius R_2 after extracting 24 carbon atoms (a); the blue circles show atoms extracted from the upper layer (b) and the bottom one (c); the hole with long size R_2 before connecting the edges by covalent bonds of corresponding pair atoms (14 such atoms of the upper layer are marked by yellow circles) in two A and B (red atoms) layers (c); view of the G_{AB} hole with 8 heptagons and 2 octagons on the oval region.

lower symmetry thus the UC has a smaller number of equivalent atoms. The mini-zones are wider then $G_{AA}\{5,h_2\}$ ones (compare Fig. 5c with Fig. 5d).

Remarks that the nanomesh $G_{AB}\{5,R_2\}$ – Fig. 5c, is a periodic structure of Y-junctions made of (4,4) CNTs[26,27] - compare it with the $G_{AA}\{5,h_2\}$ structure with hexagonal holes in Fig. 5d. Both structures are semiconductors because of potential barriers that are present in Y junctions of CNT.[47]

The meshes $G_{AB}\{L_p,R_2\}$ and $G_{AA}\{L_p,h_2\}$ with larger UC parameter L_p (p>6) will have nanotube elements with larger diameter. CNT elements with diameter D>1.5 nm should more easily be deformed in the shape of flattened CNTs through the interaction between graphene bilayers.[46] The gaps E_g of these SSs should decrease with increasing CNT diameter or the distance between neighboring holes.[26]

Hexagonal G_{AB} superlattices with «oval» closed edge holes

The «oval» holes O_q can be built in the G_{AB} bilayers when they form under an elongated spot of electron beam or with catalytic nanoparticles of oval form. We used a simple construction using connection Z edge carbon atoms (Fig. 6): 1) starting from hexagonal holes with radius $R_q=(q+1)a_{C-C}\sqrt{3}$ (q=1,2,3,…) in the layers, which were considered recently,[31] 2) excluding (1+q)4 edge atoms (see, for example, blue atoms on Fig. 6b,c in O_2 case), 3) after the atom removing, we connect the pairs of chemically active atoms, 3) than we optimize the

resulting hole O_q with short side l_q= $qa_{C-C}\sqrt{3}$ entirely of sp^2-hybridized carbon atoms to form topological defects - heptagons and octagons (see Fig. 6e).

We constructed and optimized the structure of possible nanomeshes with oval holes O_2. Fig. 6a shows AB- stacking graphene with hexagonal holes (the radius $R_2 = 3a_{C-C}\sqrt{3}$ is similar to the hole structure shown on the Fig. 1 and 2d in Ref.[31]). In Fig. 6b,c we present non bonded upper A layer (b) and bottom B layer (c) with the 4x2 atoms (blue circles) which must be removed in order to obtain oval hole O_1 with short side $l_2 \approx 2a_{C-C}\sqrt{3}$ and all sp^2 covalent bonds of corresponding 14 pair chemical active atoms (Fig. 6 d,e).

It can be possible using the same method to construct AB-stacking SS with bigger oval holes by similar transformation of non-folded hexagonal holes with bigger radius.

We denote the oval mesh as $G_{AB}(L_p, R_q)$, where $L_p \approx px3a_{C-C}$ is the lattice parameter along X axis of the superlattice, R_q and l_q are long and short sides of the oval hole (indicated by the arrows in Fig. 6).

AB bi-graphene nanomeshes are shown in Fig. 7a,d. The initially chosen hexagonal SS UCs with $L_p = p$ x3a_{C-C} (L_4 =1.7nm and L_5= 2.1nm) changed slightly after optimization to yield parallelogram unit cells with UC vectors $L_p \neq L_p$ and angle ($\mathbf{L}_p, \mathbf{L}_p$) ≠ 60° because of the less symmetry of oval holes compared to hexagonal and «round» holes (see Tabl.1). Meshes $G_{AB}(4,R_2)$ and $G_{AB}(5,2)$ have energy gaps E_g=0.5, 0.3 eV, respectively (Fig. 7b,c). If in the case of $G_{AB}(4,2)$ mesh, we have periodic Y-
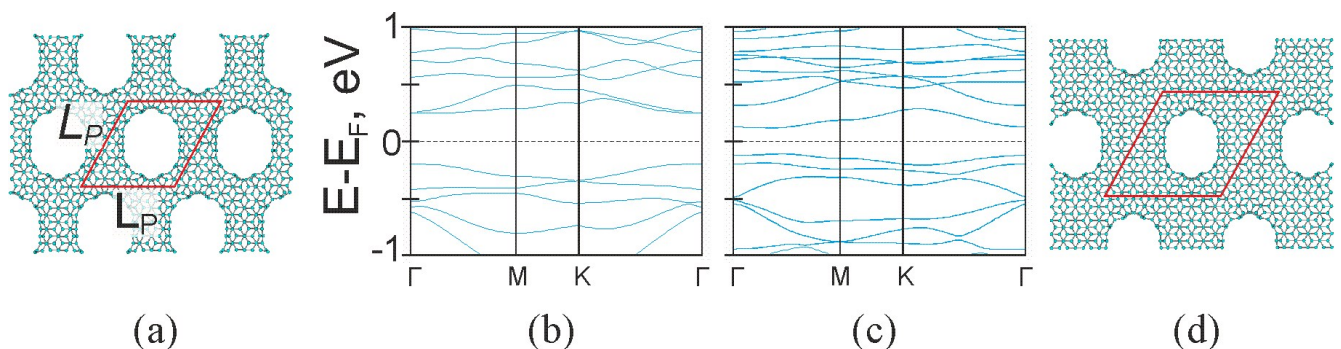
Fig. 7 Atomic and electronic band structures of AB bi-graphene hexagonal semiconductor nanomeshs with «oval» holes: $G_{AB}(4,2)$ - (a, b), G_{AB} (5,2) - (c,d), respectively.

junctions of identical (4,4) CNT fragments, characterized by a bigger band gap than for the $G_{AB}(5,2)$ mesh where the (6,6) nanotube fragments are more flattened then in the $G_{AB}(4,2)$ case. So elongated hole shape leads to semiconductor behavior of the meshes $G_{AB}(4,2)$ and $G_{AB}(5,R_2)$ due to a distinct symmetry from that of graphene like in the case of meshes $G_{AB}\{5,R_1\}$ and $G_{AB}\{5,R_2\}$ (Fig. 5b.c).

Moiré bi-graphene nanomeshes with closed edges of «hexagonal» AA and «round» AB holes

Besides AA- and AB-stacking of bilayer, infinitely many configurations can be obtained by applying a rotation of two identical lattices by an angle θ.[48] That so-called moiré bigraphene structure can be viewed as a hexagonal SS with several periodically repeating parts in which the layers are packed in different ways. The unit cell with period L(θ) consists of one AA- stacking part and two AB- stacking parts. As an example, we considered moiré biG nanomeshes with angle θ=6° and UC parameter L_5≈2.2 nm - Fig. 8.

Moiré initially chosen hexagonal SS with angle θ=6° and parameter L=2.39 nm is schematically shown in Fig. 8a. Regions where bilayer graphene arranged in AA and AB packings are clearly visible in Fig. 8a (pink and blue areas, respectively), so creation of holes is possible along the same scheme as discussed above. The atomic and electronic structures of the $G_{M6}\{5;AA2\}$ mesh are presented in Fig. 8b. In the band structure of Fig. 8(b), two crossing branch points in ΓM and ΓK regions show a metallicity of the mesh and reflects the high symmetry of corresponding SS. Some electron localization near holes leads to the formation of branches

closer to Fermi level E_F. Here, the velocities v_{Fi} in Dirac points are smaller than the value v_F of graphene, as it was also the case for the band structure of meshes $G_{AA}\{5,t_q\}$ in Fig. 4. The UC parameter of the optimized bilayer SS is slightly shorter than for the moiré pattern without holes, L=2.36 nm and the UC contains 316 atoms (N_{ext}=48). The energy per atom E/N = -155.19 eV is comparable with other nanomeshes.

Hexagons carving of the AA-stacking regions of various sizes leads to a structure consisting of Y-junction elements. Here, the nanomesh $G_{M6}\{5;AA3\}$ that would be obtained by cutting the pink areas in Fig. 8a consists of Y-type junction of (6,4)CNT fragments. Thus we have the first example of Y-junction of chiral CNTs which was not considered earlier.

Making holes is possible in the AB areas of the moiré patterns too. The construction of AA-, AB- holes combination is also possible. For example, moiré 6° mesh $G_{M6}\{5;AA2,2AB0\}$ with one hole in AA and two small holes in AB areas of their unit cell is shown on Fig. 8c. In contrast with the mesh $G_{M6}\{5;AA2\}$, this SS is metallic , is more strained and has many flat branches in its band structure - Fig. 8c.

Different GNMs with moiré structure will be studied in more details in a forthcoming paper.

Main parameters of biG nanomeshes

Table 1 lists the main parameters of the SSs considered in this paper. It is worth remarking that all the total energies E/N of the nanomeshes are found between the one of graphene and the one of CNTs, except for the case of the very strained mesh $G_{AB}(4,O_1)$. Their UC parameters are somewhat smaller than the corresponding parameters L of graphene and bi-graphene UCs.
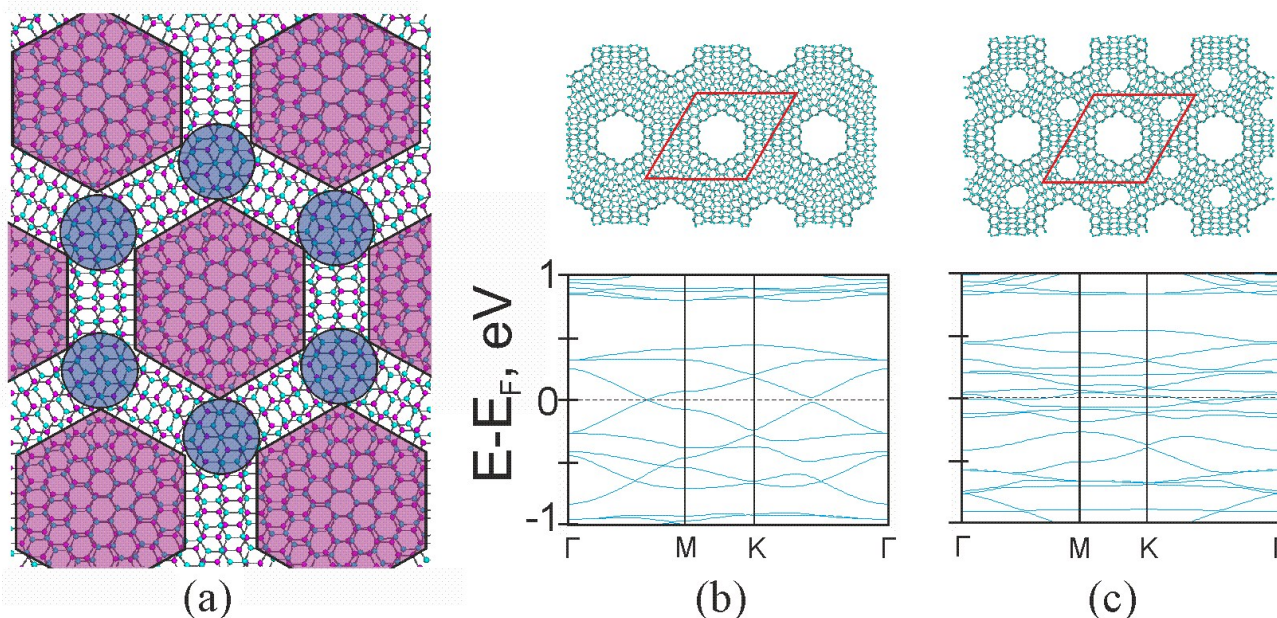
Fig. 8 Moiré graphene nanomesh structures: (a) 6° SS; pink and blue areas show areas with almost AA- and AB- stackings, respectively; (b) the nanomesh $G_{M6}\{5;AA2\}$ with one hole R_{AA2} in the center of the AA region of the hexagonal UC (red parallelogram) and its band structure; (c) the mesh $G_{M6}\{5;AA2,2AB0\}$ with the same hole R_{AA2} and two R_{AB0} holes in the center of the AB regions of the UC.

(a)   (b)   (c)
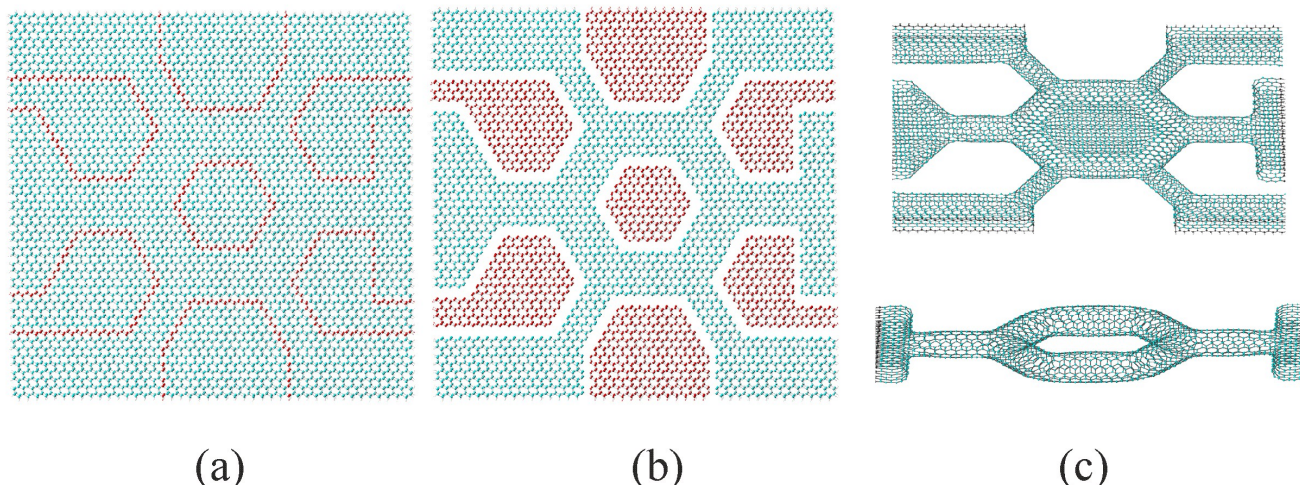
Fig. 9 Engineering of nanoelectronic elements from bilayered graphene: example of fabrication some complex mesh-like structure with four (6,6) and two (4,4)CNT terminals (a)- sketch of the biG cutting, (b) cutting – view before connection of the edges, (c) upper view is the element , «pillow trap», below view is some more simple nanoelectronic elements – Aharonov-Bohm CNT ring-like «trap».

Nanoengineering on the base bi-GSSs

Fig. 9 sketches the preparation steps and some electronic elements based on bi-graphene in the AA stacking with six CNT terminals. The borders of the future device are shown by the red lines in Fig. 9a. Electron beam exposure removes the red areas (Fig. 9b). The same procedure can be performed at a catalytic nanoparticles location on the red areas as in the case of graphene nanomeshes (for example, copper particles using[49]). Connections of the atoms occurs at the layers boundaries during such a procedure. Thus bi-graphene with six CNT terminals is formed (Fig. 9c). Using the same preparation, it is possible to conceive a structure containing two (6,6) and four (4,4) nanotubes connected with a central (6,6)CNT «ring» part (see Fig. 9b) or similar element with central «pillow» part (see Fig. 9c upper). If (4,4)CNT parts were moved away, a CNT hexagonal-like «ring» with two (6,6)CNT electrodes would be obtained. This structure looks like an Aharonov-Bohm element[50] at the nanoscale. Fig. 9 demonstrates that it is possible to prepare different nanoelectronic circuits by this method. For example, it is possible to use simplest «karigami»-like structure Fig. 9b (compare with «karigami» GNR structures in Ref.[51]). Here, the central part of the structure may be pushed away from the plane by the application of a load which leads to some stretching of the six attached long CNTs, thereby changing the electrical current in the system by applying a voltage to oppositely disposed electrodes. Similar structures can be obtained using AB or Moire bilayered graphene.

Like membrane, similar structures with nanopores can be used for filtration of gases and liquids. In another context, perforated bilayer graphene with folded edges may present interesting thermal properties, in particular zero thermal expansion[52]. Thanks to the interlayer bonds at the hole edges, the bilayer should be more rigid than with van der Waals interactions only, which should influence the flexural wave mode and, thereby, the mechanical and thermal properties of the structure[53].

Conclusions

We have performed a systematic study of a wide class of new graphene bilayer nanomesh systems with different periodic arrangements and with a large variety of hole shapes. Only a few examples have been reported in this paper. Stability and electronic properties of the modeled structures were investigated by DFT calculations. It has been shown that the zig-zag edges of the considered hexagonal holes can lead to sp^2- stitching bonds of the edges of superimposed holes, forming closed structure with perfect threefold coordination. We show that there is a rich and sometimes subtle dependence of the electronic structure of the considered systems on their geometry. The combination of quantum confinement at hole edges, the modified symmetry and periodicity due to the nanohole arrangement leads to interesting and unexpected band structures. For some symmetric cases, Dirac points typical of graphene are conserved along high-symmetry directions of the Brillouin zone. For less symmetric superstructures of bilayer nanomeshes, a semiconducting behavior is obtained. We propose also possible methods for constructing different bilayer nanoelectronic elements. Thus, our study points to the manipulation of graphene materials at the nanoscale for tailoring desirable properties.

Acknowledgements

References

1   A. Ferrari, F. Bonaccorso, V. Fal'ko, K. S. Novoselov, S. Roche, P. Bøggild, S. Borini, F. H. L. Koppens, V. Palermo, N. Pugno, J. A. Garrido, R. Sordan, A. Bianco, L. Ballerini, M. Prato, E. Lidorikis, J. Kivioja, C. Marinelli, T. Ryhänen, A. Morpurgo, J. N. Coleman, V. Nicolosi, L. Colombo, A. Fert, M. Garcia-Hernandez, A. Bachtold, G. F. Schneider, F. Guinea, C. Dekker, M. Barbone, Z. Sun, C. Galiotis, A. N. Grigorenko, G. Konstantatos, A. Kis, M. Katsnelson, L. Vandersypen, A. Loiseau, V. Morandi, D. Neumaier, E. Treossi, V. Pellegrini, M. Polini, A. Tredicucci, G. M. Williams, B. Hee Hong, J.-H. Ahn, J. Min Kim, H. Zirath, B. J. van Wees, H. van der Zant, L. Occhipinti, A. Di Matteo, I. A. Kinloch, T. Seyller, E. Quesnel, X. Feng, K. Teo, N. Rupesinghe, P. Hakonen, S. R. T. Neil, Q. Tannock, T. Löfwander and J. Kinaret, *Nanoscale*, 2015, **7**, 4598.

2   L. A. Ponomarenko, R. V. Gorbachev, G. L. Yu, D. C. Elias, R. Jalil, A. A. Patel, A. Mishchenko, A. S. Mayorov, C. R. Woods, J. R. Wallbank, M. Mucha-Kruczynski, B. A. Piot, M. Potemski, I. V. Grigorieva, K. S. Novoselov, F. Guinea, V. I. Fal'ko and A. K. Geim, *Nature*, 2013, **497**, 594.

3   T. G. Pedersen, C. Flindt, J. Pedersen, N. A. Mortensen, A.-P. Jauho and K. Pedersen, *Phys. Rev. Lett.*, 2008, **100**, 136804.

4   T. G. Pedersen, C. Flindt, J. Pedersen, A.-P. Jauho, N. A. Mortensen, and K. Pedersen, *Phys. Rev. B*, 2008, **77**, 245431.

5   L. A. Chernozatonskii, D.G. Kvashnin, O. P. Kvashnina, and N.A. Konstantinova, *J. Phys. Chem. C*, 2014, **118(2)**, 1318-1321.

6   M. Dvorak, W. Oswald and Z. Wu, *Sci. Rep.*, 2013, **3**, 2289-2295.

7   L. A. Chernozatonskii and P. B. Sorokin, J. W. Brüning, *Appl. Phys. Lett.*, 2007, **91**, 183103-183105.

8   A. K. Singh and B. I. Yakobson, *Nano Lett.*, 2009, **9**, 1540–1543.

9   M. A. Ribas, A. K. Singh, P. B. Sorokin and B. I. Yakobson, *Nano Res.*, 2011, **4**, 143-152.

10 A. H. C. Neto, F. Guinea, N. M. R. Peres, K. S. Novoselov and A. K. Geim, *Rev. Mod. Phys.*, 2009, **81**, 109–162.

11 D. C. Yu, E. M. Lupton, M. Liu, W. Liu, F. Liu, *Nano Res.*, 2008, **1**, 56–62.

12 W. Liu, Z. F. Wang, Q. W. Shi, J. Yang, and F. Liu, *Phys. Rev. B*, 2009, **80**, 233405.

13 F. Ouyang, Z. Yang, J. Xiao, D. Wu and H. Xu, *J. Phys. Chem. C*, 2010, **114**, 15578–15583.

14 F. Ouyang, S. Peng, Z. Liu and Z. Liu, *ACS Nano*, 2011, **5**, 4023-4030.

15 J. Bai, X. Zhong, S. Jiang, Y. Huang and X. Duan, *Nature Nanotech.*, 2010, **5**, 190-194.

16 M. Kim, N. S. Safron, E. Han, M. S. Arnold and P. Gopalan, *Nano Lett.*, 2010, **10**, 1125-1131.

17 J. H. Lee, Y. Jang, K. Heo, J. M. Lee, S. H. Choi, W. J. Joo, S. W. Hwang and D. Whang, *J Nanosci. Nanotech.*, 2013, **13**, 7401-7405.

18 S. N. Smirnov, I. V. Vlassiouk, R. R. Unocic, G. M. Veith, S Dai and S M. Mahurin, *Nature Nanotech.*, 2015, **10**, 459-464.

19 V. H. Nguyen, F. Mazzamuto, J. Saint-Martin, A. Bournel and P. Dollfus, *Nanotechnology,* 2012, **23**, 289502.

20 D. Choi, C. Kuru, U. Kim, G. Kim, T, Kim, R. Chen and S. Jin, *Nanoscale Research Letters*, 2015, **10**, 289.

21 G. Ning, Z. Fan, G. Wang, J. Gao, W. Qian and F. Wei, *Chem. Commun.*, 2011, **47**, 5976-5978.

22 D. Zhan, L. Liu, Y. N. Xu, Z. H. Ni, J. X. Yan, C. Zhao and Z. X. Shen, *Sci. Rep.*, 2011, **1**, 1-5.

23 A. H. C. Neto, F. Guinea, N. M. R. Peres, K. S. Novoselov and A. K. Geim, *Rev. Mod. Phys.*, 2009, **81**, 109–162.

24 L. A. Chernozatonskii and V. A. Demin, *Proceedings of the International Conference in Nanomaterials: Applicationsand Properties*, Alushta, the Crimea, 2013, pp. 03NCNN32-03NCNN34.

25 L. A. Chernozatonskii, V. A. Demin and A. A. Artyukh, A. A., *JETP Lett.*, 2014, **99**, 309–314.

26 D. G. Kvashnin, P. Vancsó, L. Yu. Antipina, G. I. Márk, L. P. Biró, P. B. Sorokin and L. A. Chernozatonskii, *Nano Research*, 2015, **8(4)**, 1250–1258.

27 L. A. Chernozatonskii, *Phys. Lett. A,* 1992, **172**, 173-176

28 A. L. Mackay and H. Terrones, *Nature,* 1991, **352**, 762.

29 T. Lenosky, X. Gonze, M. Teter and E. Vert, *Nature*, 1992, **355**, 333.

30 S. S. Gregersen, J. G. Pedersen, S. R. Power and A.-P. Jauho, *Phys. Rev. B*, 2015, **91**, 115424.

31 R. Petersen and T. G. Pedersen, *J. Phys.: Cond. Mat.*, 2015, **27**, 225502.

32 K. He, A. W. Robertson, C. Gong, C. S. Allen, Q. Xu, H. Zandbergen, J. C. Grossman, A. I. Kirklanda and J. H. Warner, *Nanoscale*, 2015, **7**, 11602-11610.

33 L. Qi, J. Y. Huang, J. Feng, J. Li, *Carbon,* 2010, **48**, 2354–2360.

34 Z. Liu, K. Suenaga, P. Harris, S. Iijima, *Phys. Rev. Lett.*, 2009, **102**, 015501.

35 J. Y. Huang, F. Ding, B. I. Yakobson, P. Lud, L. Qie, and J. Lie, *PNAS*, 2009, **106**, 10103–10108.

36 F. Börrnert, L. Fu, S. Gorantla, M. Knupfer, B. Büchner, and M. H. Rümmeli, *ACS Nano*, 2012, **6**, 10327–10334.

37 C. Thiele, A. Felten, T. J. Echtermeyer, A. C. Ferrari, C. Casiraghi, H. v. Löhneysen, R. Krupke, *Carbon*, 2013, **64**, 84–91.

38 G. Algara-Siller, A. Santana, R. Onions, M. Suyetin, J. Biskupek, E. Bichoutskaia and U. Kaiser, *Carbon*, 2013, **65**, 80–86.

39 J. M. Soler, E. Artacho, J. D. Gale, A. García, J. Junquera, P. Ordejón and D. Sánchez-Portal, *J. Phys.: Cond. Mat.*, 2002, **14**, 2745-2779

40 J. P. Perdew and A. Zunger, *Phys. Rev. B*, 1981, **23**, 5048-5079.

41 H. J. Monkhorst and J. D. Pack, *Phys. Rev. B*, 1976, **13**, 5188-5192.

42 J. P. Perdew, *Journal of Quantum Chem., 1985,* **28**, 497-503.

43 J.-K. Lee, S.-C. Lee, J.-P. Ahn, S.-C. Kim, J.I.B. Wilson and P. John, *J. Chem. Phys.*, 2008, **129**, 234709.

44 M. Vanevic, V.M. Stojanovic, M. Kindermann, *Phys. Rev. B,* 2009, **80**, 045410.

45 J. A. Fürst, T. G. Pedersen, M. Brandbyge and A.-P. Jauho, *Phys. Rev. B*, 2009, **80**, 115117.

46 P. E. Lammert, P. Zhang and V. H. Crespi, *Phys. Rev. Lett.*, 2000, **84**, 2453.

47 G. Treboux, P. Lapstun, Z. Wu and K. Silverbrook, *J. Phys. Chem. B*, 1999, **103**, 8671-8674.

48 J. M. Campanera, G. Savini, I. Suarez-Martinez and M. I. Heggie, *Phys. Rev. B*, 2007, **75**, 235449.

49 J. Liu, H. Cai, X. Yu, K. Zhang, X. Li, J. Li, N. Pan, Q. Shi, Y. Luo and X. Wang, *J. Phys. Chem. C*, 2012, **116**, 15741-15746.

50 J. S. Yoo, Y.W. Park, V. Skakalova and S. Roth, *Appl. Phys. Lett.*, 2010, **96**, 143112.

51 M. K. Blees, A. W. Barnard, P. A. Rose, S. P. Roberts, K. L. McGill, P. Y. Huang, A. R. Ruyack, J. W. Kevek, B. Kobrin, D. A. Muller and P. L. McEuen, *Nature*, 2015, **524**, 204–207.

52 A.R. Muniz and A.F. Fonseca, *J. Phys. Chem. C,* 2015, **119**, 17458–17465.

Physical Chemistry Chemical Physics Accepted Manuscript

53 J.W. Jiang, B.S. Wang, J.S. Wang and H.S. Park, *J. Phys.: Condens. Matter,* 2015, **27**, 083001 (24pp).

Structures	N, (UC atoms)	-E/N, (eV/atom)	E_g,(eV)	L, (A^o)		N_{ext}
Graphene	150	155.279	0	21.30		0
$G_{AA}t\{5, q\}$						
q=0	292	155,260	1.0	21.22		8
1	256	154.739	1.2	21.10		44
2	196	155.041	1.1	21.02		104
$G_{AA} h\{5, R_2\}$	192	155.040	0.23	21.07		108
$G_{AB} t\{5,q\}$						
q=0	292	155,266	0	21.26		8
1	256	155.177	0.2	21.25		44
2	196	155.040	0.17	20.99		104
Oval holes				L1	L2	
$G_{AB}O(4, 1)$ <(L1,L2)=118.9^o	136	154,999	0.48	16.2	16.80	56
$G_{AB} O (5, 1)$ <(L1,L2)=119.5^o	244	155.139	0.25	20.9	21.24	56
Moiré						
$G_{M6}\{5;AA2\}$	316	155.191		23.36		48
$G_{M6}\{5;AA2,2AB0\}$	300	155.027		23.24		64
(6,6)CNT	24	155.170	0			0
(4,4)CNT	16	155.021	0			0

Table. 1 Main parameters of biG nanomeshes.